INTERNATIONAL JOURNAL FOR NUMERICAL METHODS IN FLUIDS
Int. J. Numer. Meth. Fluids 2005; **48**:1351–1373
Published online 12 May 2005 in Wiley InterScience (www.interscience.wiley.com). DOI: 10.1002/fld.984

Numerical analysis on the propulsive performance and vortex shedding of fish-like travelling wavy plate

Gen-Jin Dong and Xi-Yun Lu*,†

Department of Modern Mechanics, University of Science and Technology of China, Hefei, Anhui 230026, People's Republic of China

SUMMARY

Numerical analysis is carried out to investigate viscous flow over a travelling wavy plate undergoing lateral motion in the form of a streamwise travelling wave, which is similar to the backbone undulation of swimming fish. The two-dimensional incompressible Navier–Stokes equations are solved using the finite element technique with the deforming-spatial-domain/stabilized space–time formulation. The objective of this study is to elucidate hydrodynamic features of flow structure and vortex shedding near the travelling wavy plate and to get into physical insights to the understanding of fish-like swimming mechanisms in terms of drag reduction and optimal propulsive performance. The effects of some typical parameters, including the phase speed, amplitude, and relative wavelength of travelling wavy plate, on the flow structures, the forces, and the power consumption required for the propulsive motion of the plate are analysed. These results predicted by the present numerical analysis are well consistent with the available data obtained for the wave-like swimming motion of live fish in nature. Copyright © 2005 John Wiley & Sons, Ltd.

KEY WORDS: fish-like swimming; locomotion; vortex shedding; biomechanics; travelling wavy plate; flow control; moving boundaries and interfaces; space–time finite element

1. INTRODUCTION

A biofluiddynamics of fish locomotion was founded by Lighthill with a theory for evaluating reactive forces between an undulating fish body and the water surrounding it [1, 2]. Further development of the subject was carried out and comprehensive reviews of relevant work can be found in References [3–6]. To better explore the swimming ability of these live, the wave-like swimming and flapping motions of the body are used as essential models to deal with

*Correspondence to: Xi-Yun Lu, Department of Modern Mechanics, University of Science and Technology of China, Hefei, Anhui 230026, People's Republic of China.
†E-mail: xlu@ustc.edu.cn

Contract/grant sponsor: Chinese Academy of Sciences; contract/grant number: KJCX-SW-L04
Contract/grant sponsor: National Natural Science Foundation of China; contract/grant numbers: 10332040, 10125210

Received 18 June 2004
Revised 26 March 2005
Accepted 29 March 2005

the propulsion of fish. Previously researchers have shown the ability of the caudal fin of a fish to produce a jet-like wake similar to that of a flapping foil [7–11]. While the undulating body motions produce the locomotion, it is not yet clear exactly how the body undulating motion effects the flow very near a fish or a travelling wave plate.

Usually, fish use predominant oscillatory movements [12]. Gray noted that fish swimming movement could be mainly described as a combination of two wave-like phenomena [13]. One is cyclic change of the curved shape of the body showing a lateral wave of curvature running in the caudal direction, and the other is every single point of the body performing, in consequence of the wave of lateral curvature on the body, a sinusoidal track in a horizontal plane. Thus, a travelling wavy plate problem is of interest parallel to the swimming fish, since the backbone motion of fish species is essentially similar to that of the travelling wave. This simple model is appropriate for anguilliform, subcarangiform, and carangiform swimmers [14–16].

Fish swimming can be very instructive in disclosing mechanisms of unsteady flow control, which was raised first in the relation to swimming of live fish. Gray [17] observed that an actively swimming dolphin only consumes one seventh of the energy needed to tow a rigid body at the same speed, and suggested that substantial drag reduction must occur in the live dolphin. Then, much work has been performed to explore this problem. Important contributions by Lighthill [1, 2] and Wu [18, 19] have shed light on the inviscid hydrodynamics of fish-like propulsion. Cheng *et al.* [20] analysed the swimming propulsion mechanism of a three-dimensional plate moving in an inviscid fluid. Furthermore, Harper and Blake [21, 22] reported experimentally the outstanding performance by fish and led to interest in fish-like vehicles capable of emulating the high performance of fish propulsion and maneuvering. Barrett *et al.* [23] found that the power required to propel a swimming body may be smaller than that needed to tow a straight-rigid body.

It has been proposed that the travelling wave motions result in reducing drag force and increasing propulsive efficiency by restraining separation [24–26]. Viscous flow past a travelling wavy wall, in which the wall wavy displacements propagate in the streamwise direction, differs from the flow near a fixed wavy wall. The flow over the wavy wall is strongly affected by surface normal pressure gradient and centrifugal force due to alternating convex and concave curvatures. The effects of a surface normal pressure gradient are evident as the flow over a rotationally oscillating cylinder, in which flow separation can be reduced as observed experimentally by Tokumaru and Dimotakis [27], and numerically by Lu and Sato [28] and Lu [29]. Experiments were undertaken to investigate viscous flow past a travelling wavy wall. Taneda and Tomonari [30] observed that the boundary layer separates at the back of the wave crest for the travelling wave phase speed being smaller than the external flow velocity, but the boundary layer does not separate for the wave phase speed being larger than the external flow velocity. Kendall [31] investigated the effect of a travelling wavy wall on flow behaviour. Numerical simulations [32, 33] have been carried out for viscous flow over a fixed wavy surface and confirmed the previous experimental measurements.

To understand fish swimming propulsion, it is needed to study two typical problems which consist of the nature of the force resisting the motion and the mechanisms that lead to the thrust force [25, 26]. Here, computational fluid dynamics is applied to investigate viscous flow over a travelling wavy plate undergoing lateral motion in the form of a streamwise travelling wave. To the best of our knowledge, the relevant problem has never been examined. Meanwhile, we recognize the somewhat limitation of this model for modelling fish swimming; however,

still feel that the results will be of fundamental use in exploring the hydrodynamic feature of the flow near the travelling wavy plate and in getting into physical understanding of fish-like swimming mechanisms.

This paper is organized as follows. The physical problem and mathematical formulations are described in Section 2. The numerical method and its validation are briefly given in Section 3. In Section 4, the flow structures, forces and power consumption are discussed. Finally, concluding remarks are summarized in Section 5.

2. PHYSICAL PROBLEM AND MATHEMATICAL FORMULATION

As shown in Figure 1(a), viscous flow over a moving plate undergoing a travelling wave motion is considered. The two-dimensional incompressible Navier–Stokes equations are employed as governing equations. To non-dimensionalize the equations, the length of the wavy plate L is used as the length scale, and the free-stream velocity U as the velocity scale. Then, the non-dimensional equations are given as

$$\frac{\partial u_i}{\partial x_i} = 0 \tag{1}$$

$$\frac{\partial u_i}{\partial t} + \frac{\partial}{\partial x_j}(u_i u_j) = -\frac{\partial p}{\partial x_i} + \frac{1}{Re}\nabla^2 u_i \tag{2}$$

where Re is the Reynolds number defined as $Re = UL/\nu$ with ν being the kinematic viscosity. The pressure p is normalized by ρU^2 where ρ is the fluid density.

The wavy plate is taking a vertical oscillation in the form of a wave travelling in the streamwise direction, and the non-dimensional position of the wall is described as

$$y_w = A_m(x)\cos[2\pi\alpha(x - ct)], \quad 0 \leqslant x \leqslant 1 \tag{3}$$

where $\alpha = L/\lambda$ with λ being the wavelength of travelling wave, A_m and c are the amplitude and the phase speed of travelling wave, and subscript w denotes the quantity on the wall.

Note that the amplitude $A_m(x)$ is a function of x $(0 \leqslant x \leqslant 1)$. Here, two typical cases are considered. One is the travelling wavy plate with uniform amplitude, i.e. the amplitude being

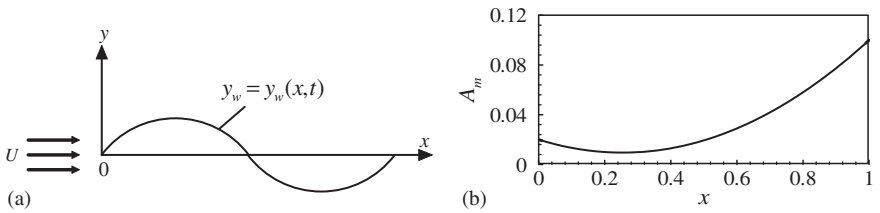

Figure 1. (a) Sketch of the physical problem; and (b) the amplitude distributions $A_m(x)$ based on the kinematic data of a steadily swimming saithe.

independent of x

$$A_m(x) = \text{constant} \tag{4a}$$

and the other is the amplitude varying with x. To model the backbone undulation of fish swimming [34], the amplitude $A_m(x)$ is approximated to be in the form of quadratic polynomial and written as

$$A_m(x) = C_0 + C_1 x + C_2 x^2 \tag{4b}$$

where C_0, C_1 and C_2 are coefficients and can be determined by the following conditions:

$$A_m(0) = 0.02, \quad A_m(0.2) = 0.01 \quad \text{and} \quad A_m(1) = 0.1 \tag{4c}$$

It is necessary to indicate that those three typical points are cited from the kinematic data of a steadily swimming saithe [34]. The amplitude $A_m(x)$ is plotted in Figure 1(b) and reasonably represents the lateral motion of the backbone undulation of fish swimming.

In the present study, an inertia frame is chosen. The travelling wavy plate is treated as a moving boundary. On the surface of the plate, fluid elements move with the travelling wavy plate described in Equation (3), and $\partial u_i/\partial \mathbf{n} = 0$ is employed on the upper and lower far-boundary with $\mathbf{n}$ being the unit vector normal to the boundary. Uniform flow is set on the inflow boundary, and the normal and shear stress are specified to be zero at the downstream outflow boundary.

3. NUMERICAL METHOD AND VALIDATION

To deal with the moving plate and the deformation of the mesh, the space–time finite element formulation, which is described in detail in Reference [35], is used in the present study. To ensure the computation stability, the series of element-level integrals are added to the conventional Galerkin formulation as the least-squares terms. This type of stabilization is referred to as the Galerkin/least-squares (GLS) procedure and is a generalization of the streamline-upwind/Petrov–Galerkin (SUPG) [36] and pressure-stabilization/Petrov–Galerkin (PSPG) [37]. Equal-in-order basis functions for the velocity and pressure, which are bilinear in space and linear in time, are used, and the Gaussian quadrature is employed for numerical integration [38]. The nonlinear equations resulting from the finite-element discretization of the equations are solved by Newton–GMRES method [39].

In the present study, to adapt the travelling wavy plate, the deformation of mesh is used. As shown in Figure 1(a), the computational domain is from -1 to 15 along the longitudinal (or streamwise) direction (i.e. x-direction) and -4 to 4 along the transverse direction (i.e. y-direction). The element number is around 2×10^4 and the time step is 0.005.

Extensive convergence checks have been taken in our previous work [40, 41]. As a typical case, Figure 2 shows the distributions of the pressure and vorticity over the upper surface of the wavy plate at $t/T = 0$ and $1/4$, and the time-dependent drag and lateral force coefficients, calculated by different element numbers, time steps and domain sizes. The results obtained by different computational conditions agree well with each other. It can be confirmed that the computed results are independent of the time step, the grid size and the computational domain size.

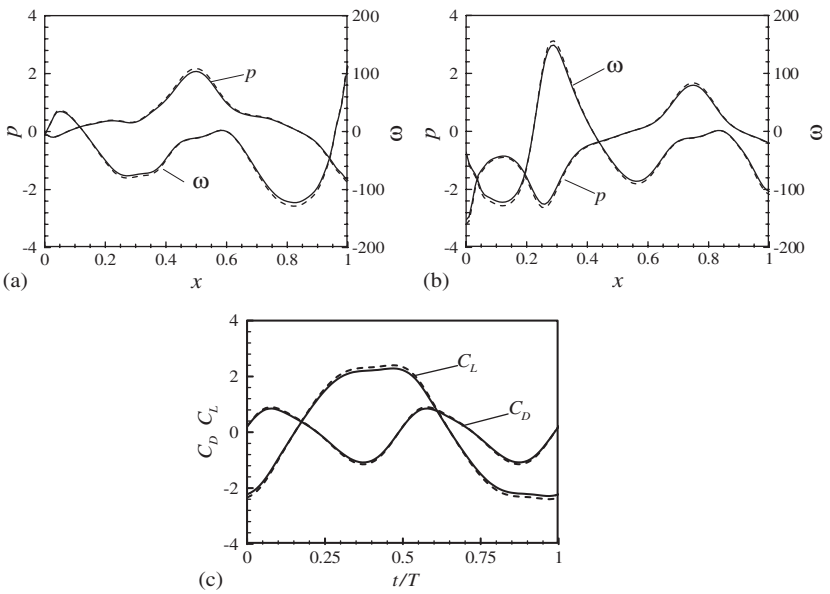

Figure 2. Validation for a travelling wavy plate with uniform amplitude at $c = 1.5$, $\alpha = 1$, $A_m = 0.3$ and $Re = 500$: Distributions of the pressure and vorticity over the upper surface of the wavy plate at: (a) $t/T = 0$; and (b) 1/4; and (c) the time-dependent drag and lateral force coefficients. Solid lines: element number around 2×10^4, time step 0.005, domain $[-1, 15]$ in the x-direction and $[-4, 4]$ in the y-direction; dashed lines: element number around 4.8×10^4, time step 0.0025, domain $[-2, 25]$ in the x-direction and $[-6, 6]$ in the y-direction.

4. RESULTS AND DISCUSSION

To investigate systematically the mechanism of propulsive performance and vortex shedding of a travelling wavy plate, the parameters are chosen as follows. The phase speed c ranges from 0.5 to 2.5. The ratio of the length of wavy plate and the travelling wavelength $\alpha = L/\lambda$ is 0.8–1.2. The uniform amplitude A_m in Equation (4a) is from 0.03 to 0.3; and the non-uniform amplitude given by Equation (4b) with the maximum trailing-edge amplitude 0.1 is shown in Figure 1(b). According to the relevant work on the motion of an aquatic animal at intermediate Reynolds numbers (i.e. $Re \sim O(10^2)$) [42], the Reynolds number is chosen as 500.

4.1. Forces and power consumption for different phase speeds

The drag force acting on the wavy plate and the power needed for it to be propelled are directly relevant to the study of fish locomotion. The total drag force on the wavy plate consists of a friction drag and a form drag due to pressure distribution. In Figure 1(a), for an element of the plate along its upper side $\mathrm{d}s = [1 + (\mathrm{d}y_w/\mathrm{d}x)^2]^{1/2}$, its tangential direction is $\mathbf{t} = (1, \mathrm{d}y_w/\mathrm{d}x)/\mathrm{d}s$ and the wall-normal direction is $\mathbf{n} = (-\mathrm{d}y_w/\mathrm{d}x, 1)/\mathrm{d}s$. Then, the friction

force and the pressure force per unit length along the wavy plate can be expressed as [25, 26]

$$\begin{cases} f_x^{\mathrm{f}} = \dfrac{1}{Re}\left[-2\dfrac{\partial u}{\partial x}\dfrac{\mathrm{d}y_{\mathrm{w}}}{\mathrm{d}x} + \left(\dfrac{\partial v}{\partial x} + \dfrac{\partial u}{\partial y}\right)\right] \\ f_x^{\mathrm{p}} = p\dfrac{\mathrm{d}y_{\mathrm{w}}}{\mathrm{d}x} \end{cases} \quad \text{on } y = y_{\mathrm{w}}^{+} \tag{5a}$$

$$\begin{cases} f_x^{\mathrm{f}} = \dfrac{1}{Re}\left[2\dfrac{\partial u}{\partial x}\dfrac{\mathrm{d}y_{\mathrm{w}}}{\mathrm{d}x} - \left(\dfrac{\partial v}{\partial x} + \dfrac{\partial u}{\partial y}\right)\right] \\ f_x^{\mathrm{p}} = -p\dfrac{\mathrm{d}y_{\mathrm{w}}}{\mathrm{d}x} \end{cases} \quad \text{on } y = y_{\mathrm{w}}^{-} \tag{5b}$$

where y_{w}^{+} and y_{w}^{-} represent the upper and lower surface of the wavy plate, respectively. By performing integration of f_x^{f} and f_x^{p} over both the side of plate, the friction force F_{f}, the pressure force F_{p}, and the total drag force $F_{\mathrm{d}} = F_{\mathrm{f}} + F_{\mathrm{p}}$ can be obtained. The corresponding drag coefficients are defined as

$$C_{\mathrm{DF}} = \frac{F_{\mathrm{f}}}{1/2\rho U^2 L}, \quad C_{\mathrm{DP}} = \frac{F_{\mathrm{p}}}{1/2\rho U^2 L}, \quad C_{\mathrm{D}} = \frac{F_{\mathrm{d}}}{1/2\rho U^2 L} \tag{6}$$

Based on the definition [25, 26], the total power (P_{T}) required for the propulsive motion of the wall consists of two parts. One is the swimming power, required to produce the vertical oscillation of travelling wave motion, and is defined as

$$P_{\mathrm{S}} = \int_0^L \left[(p_+ - p_-)\frac{\mathrm{d}y_{\mathrm{w}}}{\mathrm{d}t}\right]\mathrm{d}x \tag{7}$$

where p_+ and p_- are the pressure on the upper and lower surface of the plate. The other is the power, needed to overcome the drag force, and is represented as $P_{\mathrm{D}} = UF_{\mathrm{d}}$. Thus, the total power $P_{\mathrm{T}} = P_{\mathrm{S}} + P_{\mathrm{D}}$ is obtained.

The time-averaged drag force versus c at $A_m = 0.1$ and $\alpha = 1$ is shown in Figure 3(a). With the increase of c, the time-averaged form drag coefficient ($\bar{C}_{\mathrm{DP}}$) and total drag coefficient

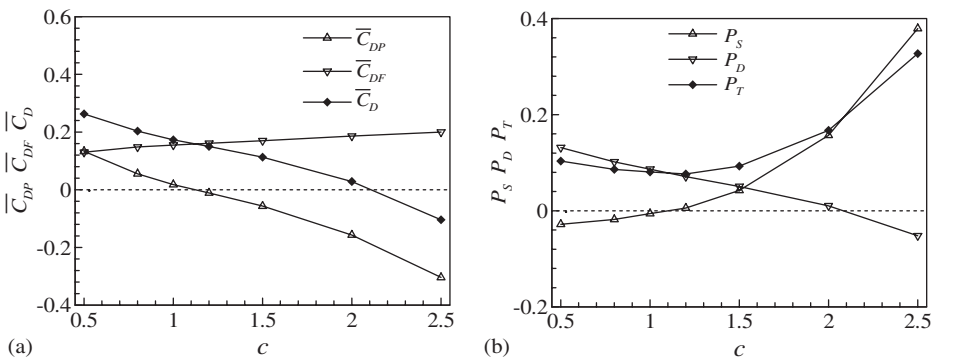

Figure 3. Time-averaged drag force and power consumption versus c at $A_m = 0.1$ and $\alpha = 1$: (a) drag force acting on the travelling wavy plate; and (b) power required to propel the wavy plate.

($\bar{C}_D$) decrease, and the friction drag coefficient ($\bar{C}_{DF}$) increases somewhat. It is noted that $\bar{C}_{DP}$ becomes negative and acts as thrust force when $c>1$ approximately, and $\bar{C}_D$ gets negative when $c>2$ approximately. This behaviour is consistent with previous findings for viscous flow over a streamwise travelling wavy wall [25, 26].

The distributions of P_T, P_S and P_D are shown in Figure 3(b). As c increases, P_S increases and becomes positive for $c>1$ approximately. The negative value of P_S means that the wavy plate motion can be actuated by the flow and no power input is needed. The power to overcome the drag force, P_D, decreases monotonically with c, because of the similar decrease of $\bar{C}_D$, as shown in Figure 3(a). When P_D is negative, it means that the wavy plate is propelled by the thrust; however, the thrust is at the expense of the swimming power P_S required to produce the plate motion. P_D and P_S present the competing mechanisms. The distribution of total power P_T versus c is concave upwards with a minimum around $c=1.2$, which is consistent with the value used for travelling wave-like swimming motion of live fish in nature [43, 44].

To elucidate the behaviour of time-dependent drag forces, Figure 4 shows the drag coefficients for several phase speeds at $A_m=0.1$. It is needed to indicate that, based on our calculated results, periodic results are obtained for all the cases considered here. Thus, to clearly exhibit time-dependent drag forces, the results during one cycle are only shown in Figure 4. It is noted that the time-dependent friction drag is nearly constant during the cycle; the time-dependent form drag is always positive at $c=0.5$ and 0.8 in Figures 3(a) and (b), and becomes alternately positive and negative for $c\geqslant 1$. When the form drag becomes negative, it acts as a thrust force. The form drag plays an essential role for the propulsion of the travelling wavy plate.

It is reasonably predicted that two peaks of time-dependent drag force are generated during one cycle, because two vortices with opposite sign shed into the wake of the plate and the corresponding vorticity structures are shown later. Further, by examining the time (or phase) corresponding to the peak of form drag C_{DP} marked by '$\times$' in Figure 4, the profile of the time (or phase) versus c is obtained and exhibited in Figure 5. It is interesting to note that the time (or phase) has a sharp change from $t/T=0.4$ (or phase $\phi=4\pi/5$) when $c<1$ approximately to $t/T=0.6$ (or $\phi=6\pi/5$) when $c>1$. This feature is consistent with the variation of $\bar{C}_{DP}$ in Figure 3(a), where $\bar{C}_{DP}$ changes from positive for $c<1$ approximately to negative for $c>1$.

Time-dependent lateral force coefficient (C_L) and the root-mean-square (rms) values of drag and lateral force (i.e. C_{Drms} and C_{Lrms}) are shown in Figures 6(a) and 6(b). When c increases, the amplitude of time-dependent C_L increases in Figure 6(a), and the corresponding C_{Lrms} increases in Figure 6(b). However, note that C_{Drms} reaches a minimum at $c=1$; C_{Drms} decreases somewhat for c increasing from 0.5 to 1, and increases quickly for c increasing from 1 to 2.5.

4.2. Flow structures for different phase speeds

To elucidate the effect of c on the form drag force, Figure 7 shows the pressure contours for several phase speeds. At $c=0.5$ (in Figure 7(a)), lower pressure distribution along the wavy plate of the right side of the crest appears; thus the form drag is always positive during the cycle shown in Figure 4(a). When $c\geqslant 1$ approximately, the pressure patterns exhibit a remarkable change. It is noted that larger pressure distribution appears over the trough region and lower pressure over the crest region. The form drag varies with positive and negative

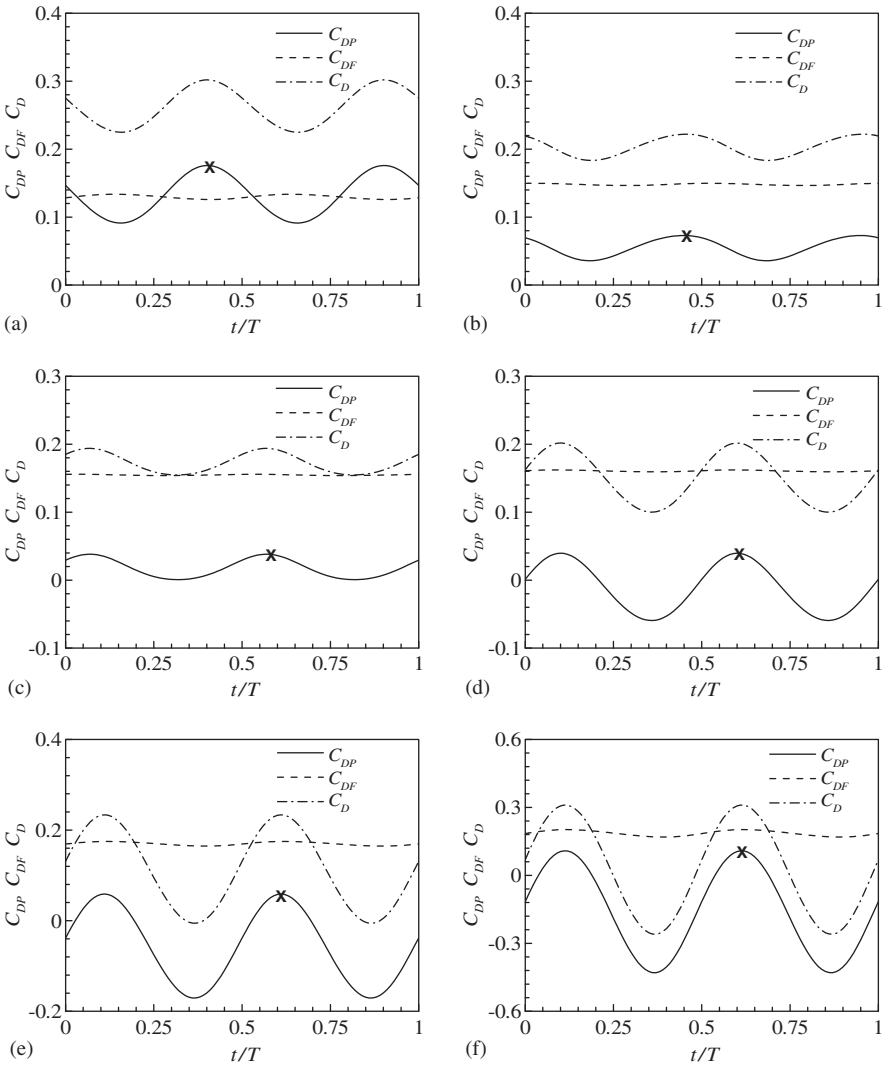

Figure 4. Time-dependent friction drag (C_{DF}), form drag (C_{DP}) and total drag (C_{D}) for $A_m = 0.1$ and $\alpha = 1$ with several phase speeds: (a) $c = 0.5$; (b) 0.8; (c) 1.0; (d) 1.2; (e) 1.5; and (f) 2.0.

values during the cycle, e.g. $c = 1.5$ and 2 in Figures 4(e) and 4(f). Thus, it is reasonably predicted that the time-averaged form drag ($\bar{C}_{\mathrm{DP}}$) decreases with the increase of c and becomes negative for $c > 1$ in Figure 3(a), and the time (or phase) corresponding to the peak of form drag exhibits a jump around $c = 1$ in Figure 5.

The corresponding instantaneous streamline patterns are shown in Figure 8. As the wavy plate is travelling in the streamwise direction, the plate boundary is no longer a streamline and there are streamlines that emanate from the plate and end on the plate. As the plate waving motion, the right side of the crest rises and the left side descends, and the vertical

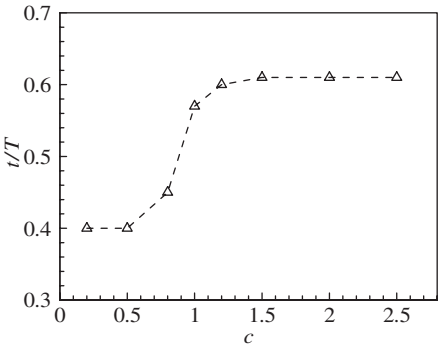

Figure 5. Profile of the time (or phase) versus c at $A_m = 0.1$ and $\alpha = 1$.

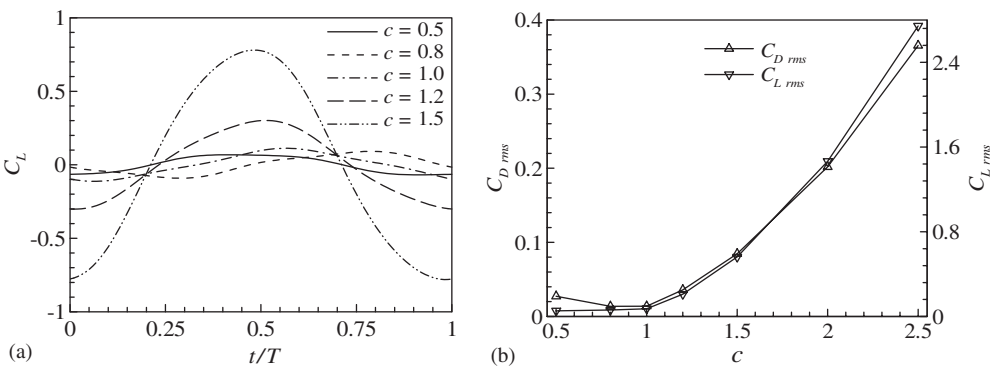

Figure 6. Profiles of the lateral force (C_{L}) and the root-mean-square values of drag and lateral force (C_{Drms} and C_{Lrms}) at $A_m = 0.1$ and $\alpha = 1$: (a) C_{L}; and (b) C_{Drms}, C_{Lrms}.

flow induced increases with the increase of c. As a result, while the streamlines above the trough are concave at $c = 0.5$, they become flat at $c = 1$ approximately and even convex at $c = 1.5$ and 2. It is well known that the flow over the wavy plate is strongly affected by surface normal pressure gradient and centrifugal force due to alternating convex and concave curvatures. Thus, the convex streamlines over the trough at $c = 1.5$ and 2 in Figures 8(c) and 8(d) agree reasonably with the larger pressure distributions over the trough region in Figures 7(c) and 7(d). The surface normal pressure gradient increases with c. As the lateral force is contributed mainly by the pressure distribution, it is reasonably noted that the amplitude of time-dependent C_{L} increases and the corresponding C_{Lrms} increases in Figure 6.

The plate travelling wave motion tends to suppress flow separation along the plate. As well studied, the effects of a surface normal pressure gradient are evident as the flow over a rotationally oscillating cylinder, in which flow separation can be reduced as verified experimentally by Tokumaru and Dimotakis [27], and numerically by Lu and Sato [28] and Lu [29]. Thus, as described above, the effect of the surface normal pressure gradient when $c > 1$ approximately is a mechanism for the suppression of flow separation along the plate, in

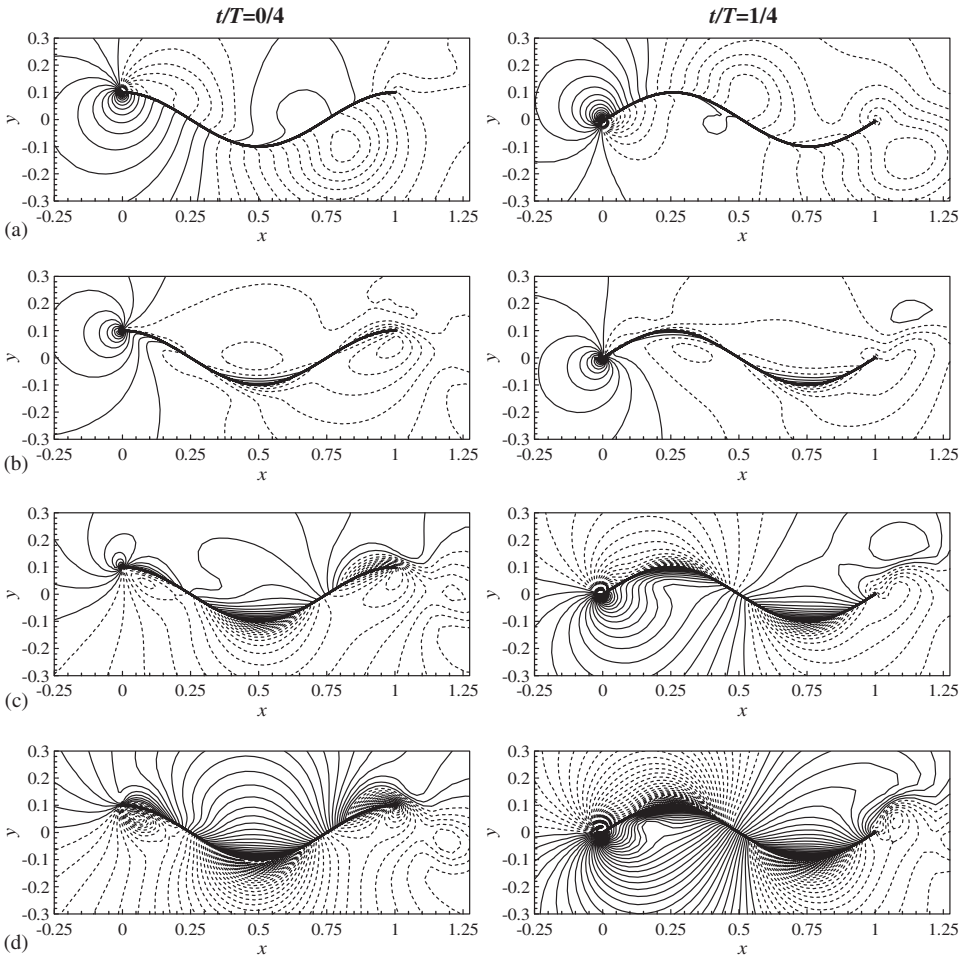

Figure 7. Instantaneous pressure contours for $A_m = 0.1$ and $\alpha = 1$ at $t/T = 0/4$ (left column) and $1/4$ (right column): (a) $c = 0.5$; (b) 1.0; (c) 1.5; and (d) 2.0.

particular in the region of the crest. Based on our results and previous findings [25, 26], it is confirmed that the flow separation over a travelling wavy wall is effectively restrained for $c > 1$.

To understand propulsive performance of the travelling wavy plate, vortex structures in the near wake of the plate are discussed. Unlike previous work for infinite travelling wall [25, 26, 31–33], we can deal with the vortex structures in the near wake of the plate. Figure 9 shows the vorticity contours at $c = 0.5$ during one cycle. The shear layer is generated along the plate and rolls up to form concentrated vortices behind the crest. Then, the vortices gradually shed into the downstream to form vortices array, similar to classic Karman vortex-street in the near wake of the travelling wavy plat. It is noted that two vortices with opposite sign shed downstream during one cycle. By comparing the vorticity structures between $t/T = 0/4$ and

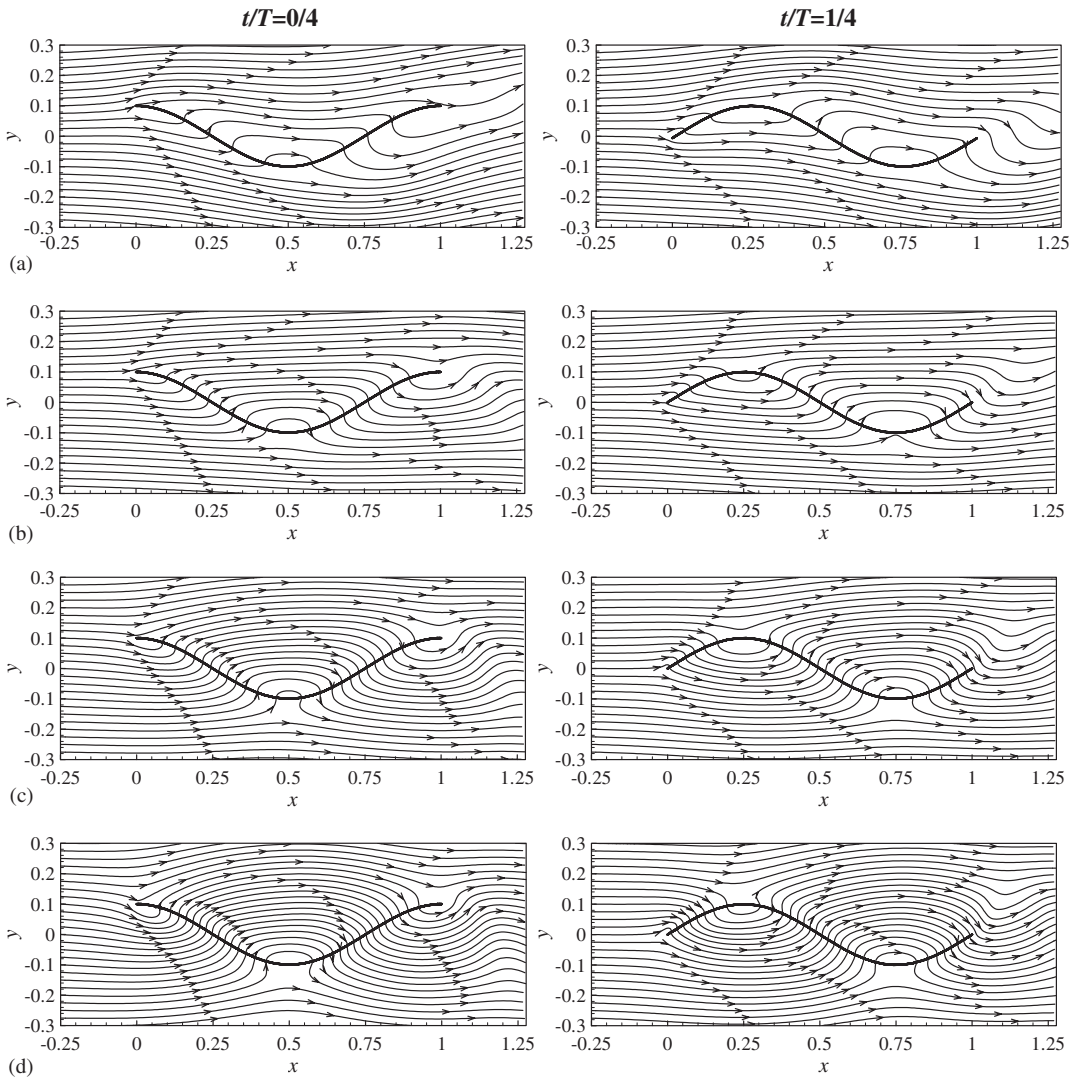

Figure 8. Instantaneous streamline patterns for $A_m = 0.1$ and $\alpha = 1$ at $t/T = 0/4$ (left column) and $1/4$ (right column): (a) $c = 0.5$; (b) 1.0; (c) 1.5; and (d) 2.0.

$2/4$ (and between $t/T = 1/4$ and $3/4$) in Figure 9, as expected, the patterns appear reasonably antisymmetric.

Figure 10 shows the vorticity contours at $t/T = 0/4$ and $1/4$ for several phase speeds. With the increase of c, the scale of shedding vortex and the lateral width of the vortices array in the near wake decrease gradually, even a vortex-street ranking near as one line at $c = 2$ and 2.5. It is also observed that the vortex-street can keep its structure up to a long distance in the downstream of the plate at $c = 0.5$ and 0.8. However, when $c \geqslant 1$, the vortex-street dissipates

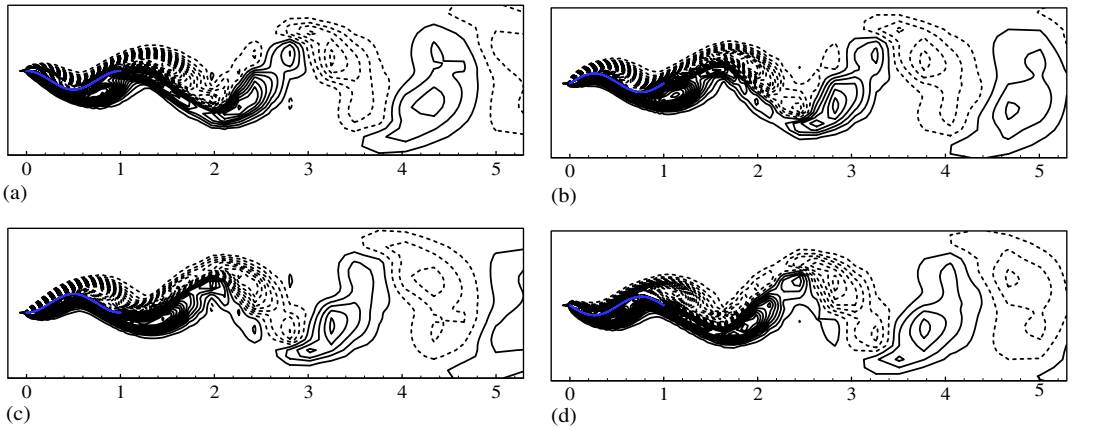

Figure 9. Vorticity contours for $c = 0.5$, $A_m = 0.1$ and $\alpha = 1$ during one cycle: (a) $t/T = 0/4$; (b) 1/4; (c) 2/4; and (d) 3/4.

quickly and even disappears nearly, e.g. for $x > 3.5$ approximately at $c = 1.2$, $x > 2.5$ at $c = 2$, and $x > 2$ at $c = 2.5$. Thus, it is reasonably identified that the vortex-street shed from the plate, which takes a travelling wave motion, tends to be dissipated effectively with the increase of c. This behaviour is consistent with the decrease of the drag force shown in Figure 3a.

4.3. *Effect of amplitude on forces, power consumption and flow structures*

To deal with the effect of the amplitude of travelling wavy plate on the forces and flow structures, the travelling wavy plate with uniform amplitude is considered. Here, some typical results are analysed for $c = 1.5$, because the phase speed value employed for travelling wave-like swimming motion of live fish in nature is $c = 1.2$–1.5 approximately [34, 43].

Figure 11 shows the time-averaged drag force and power for $c = 1.5$ and $\alpha = 1$. When A_m increases, $\bar{C}_{\mathrm{DF}}$ increases somewhat, $\bar{C}_{\mathrm{DP}}$ and $\bar{C}_{\mathrm{D}}$ decrease in Figure 11(a). It is noted that $\bar{C}_{\mathrm{D}}$ becomes negative around $A_m = 0.2$. As shown in Figure 11(b) for P_{T}, P_{S} and P_{D}, when A_m increases, P_{S} and P_{T} increase and P_{D} decreases. At larger amplitude, e.g. at $A_m = 0.3$, P_{D} becomes negative; it means that the wavy plate is propelled by the thrust. However, the thrust is at the expense of the swimming power P_{S} required to produce the wavy plate motion. On the other hand, at smaller amplitude, e.g. at $A_m = 0.05$, it is noted that, although the swimming power P_{S} is small, the form drag hardly produces enough thrust force at small A_m. Thus, it is reasonably proposed that there exist optimal amplitudes to generate a high propulsive efficiency for the travelling wavy plate [26]. As shown in Figure 11(c) for the rms values of drag and lateral force, it is reasonably predicted that C_{Drms} and C_{Lrms} increase with the increase of A_m.

Figure 12 shows the instantaneous streamline patterns and pressure contours at $A_m = 0.05$ and 0.2. The vertical flow induced by the plate waving motion increases with the increase of A_m. It is evident that, comparing with the patterns at $A_m = 0.05$, the streamlines above the trough become remarkably convex at $A_m = 0.2$. Thus, in Figures 11(b) and 11(d), the surface

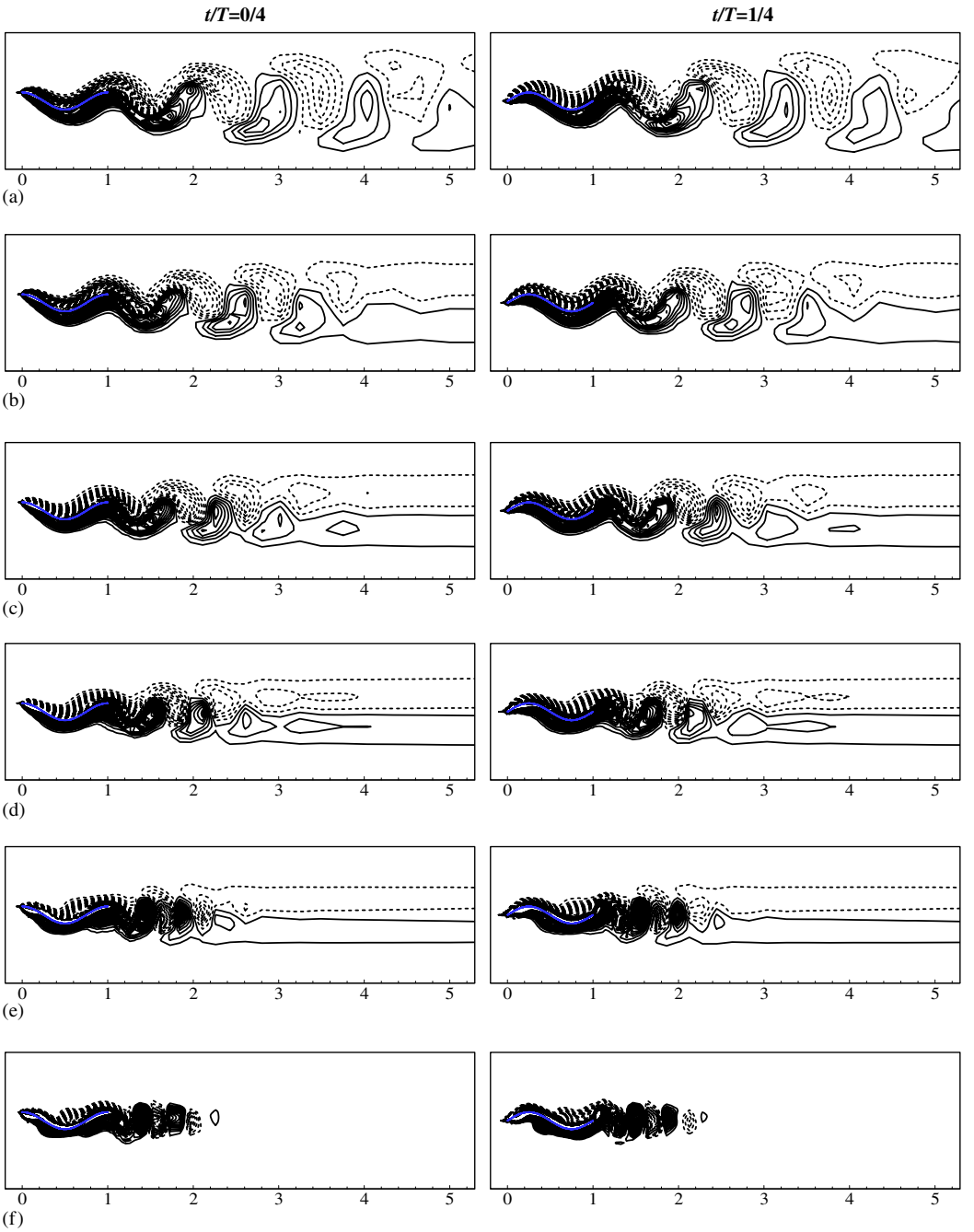

Figure 10. Vorticity contours for $A_m = 0.1$ and $\alpha = 1$ at $t/T = 0/4$ (left column) and $1/4$ (right column): (a) $c = 0.8$; (b) 1.0; (c) 1.2; (d) 1.5; (e) 2.0; and (f) 2.5.

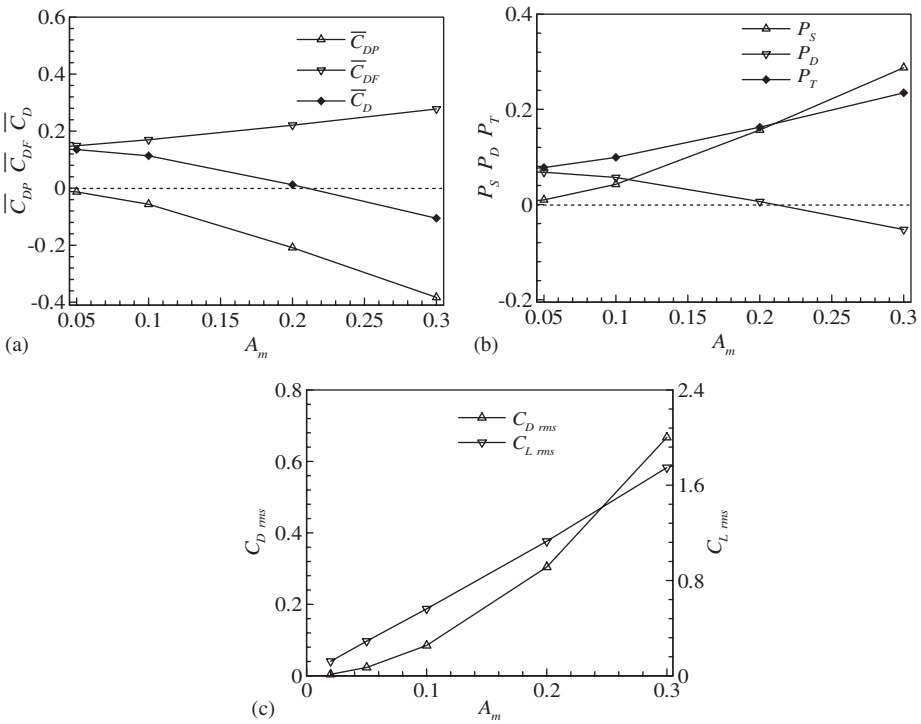

Figure 11. Time-averaged drag force and power consumption, and the rms values of drag and lateral forces at $c = 1.5$ and $\alpha = 1$: (a) drag force; (b) power consumption; and (c) C_{Drms}, C_{Lrms}.

normal pressure gradient increases with A_m to balance the centrifugal force induced by the convex streamlines over the trough.

4.4. *Effect of relative wavelength on forces, power consumption and flow structures*

The effect of the relative wavelength, which can be represented by the ratio between the length of the wavy plate and the travelling wavelength (i.e. $\alpha = L/\lambda$), on the forces and flow structures is studied. The relative wavelength α is typically chosen as 0.8 to 1.2 for the travelling wavy plate with uniform amplitude.

The time-averaged drag force and power versus α are shown in Figure 13. As α increases, $\bar{C}_{\mathrm{DF}}$ increases, $\bar{C}_{\mathrm{DP}}$ decreases, and $\bar{C}_{\mathrm{D}}$ decreases somewhat in Figure 13(a); P_{s} increases, P_{d} decreases, and P_{T} increases in Figure 13(b). The changes of the drag force and power induced by α, compared to these caused by the phase speed c and the amplitude A_m in Figures 3 and 11, are relatively small. The rms values of drag and lateral force are shown in Figure 13(c). As α increases from 0.8 to 1.2, C_{Lrms} decreases monotonically; however, C_{Drms} appears a maximum at $\alpha = 1$.

Figure 14 shows the streamline patterns and pressure contours for $\alpha = 0.8$ and 1.2. At $t/T = 0/4$, two wave troughs are formed at $x = 0.415$ (viewing on the upper side of the plate) and 0.83 (on the lower side) approximately for $\alpha = 1.2$, but only one wave trough on the upper

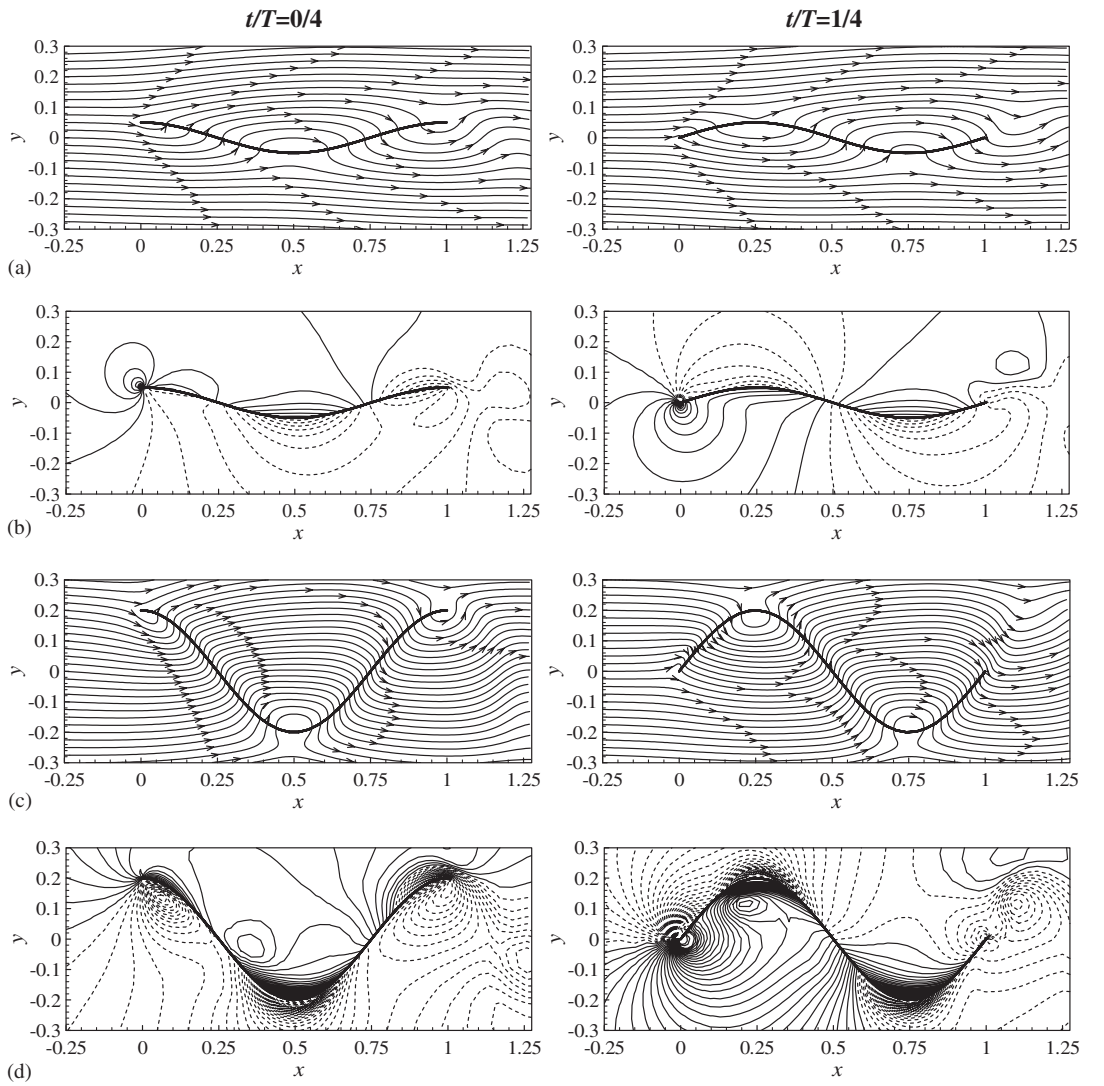

Figure 12. Instantaneous streamlines and pressure contours for $c = 1.5$ and $\alpha = 1$ at $t/T = 0/4$ (left column) and $1/4$ (right column): (a) streamlines at $A_m = 0.05$; (b) pressure contours at $A_m = 0.05$; (c) streamlines at $A_m = 0.2$; and (d) pressure contours at $A_m = 0.2$.

side of the plate appears at $x = 0.625$ for $\alpha = 0.8$. As the effect of the surface normal pressure gradient, the larger pressure distributions over the trough region occur, as shown in Figures 14(b) and 14(d). The lateral force is mainly contributed by the pressure and is closely related to the pressure distributions over both the sides of the plate. Thus, the pressure distributions on both the sides of the plate are effectively balanced at $\alpha = 1.2$, caused that C_{Lrms} quickly decreases with α in Figure 13(c).

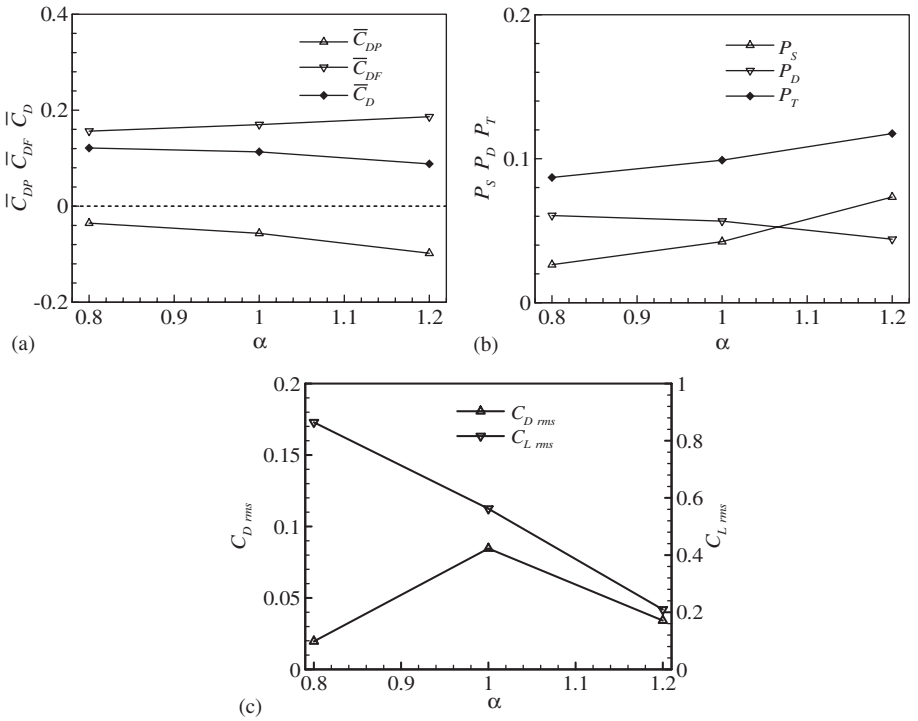

Figure 13. Time-averaged drag force and power consumption, and the rms values of drag and lateral forces at $c = 1.5$ and $A_m = 0.1$: (a) drag force; (b) power consumption; and (c) C_{Drms}, C_{Lrms}.

4.5. Effect of non-uniform amplitude on forces, power consumption and flow structures

Based on the kinematic data of steadily swimming fish, the backbone undulation of fish swimming is physically described by travelling waves of lateral curvature with increasing amplitude. Therefore, the effect of non-uniform amplitude on the forces and flow structures is analysed. The amplitude $A_m(x)$ is shown in Figure 1(b), where the amplitude at the trailing-edge of the plate (i.e. at $x = 1$) is 0.1.

Figure 15 shows the time-averaged drag force and power consumption. When c increases, $\bar{C}_{\mathrm{DP}}$ and $\bar{C}_{\mathrm{D}}$ decrease, and $\bar{C}_{\mathrm{DF}}$ increases. In Figure 15(a), $\bar{C}_{\mathrm{DP}}$ becomes negative and acts as thrust force when $c > 0.8$ approximately. Comparing with Figure 3(a), it is noted that $\bar{C}_{\mathrm{DP}}$ for non-uniform amplitude is smaller than that for uniform amplitude in Figure 3(a) at the same c. Thus, it is reasonably predicted that the travelling wavy plate with non-uniform amplitude is helpful to generate effectively a thrust. Actually, the travelling waves with increasing amplitude are a typical form adopted for travelling wave-like swimming motion of live fish in nature.

As shown in Figure 15(b), when c increases, P_{S} increases. P_{S} becomes positive for $c > 0.8$ approximately. The power to overcome the drag force, P_{D}, decreases monotonically with c. The distribution of P_{T} versus c is concave upwards with a minimum around $c = 1.2$. The rms values of drag and lateral force are exhibited in Figure 15(c). When c increases, C_{Lrms}

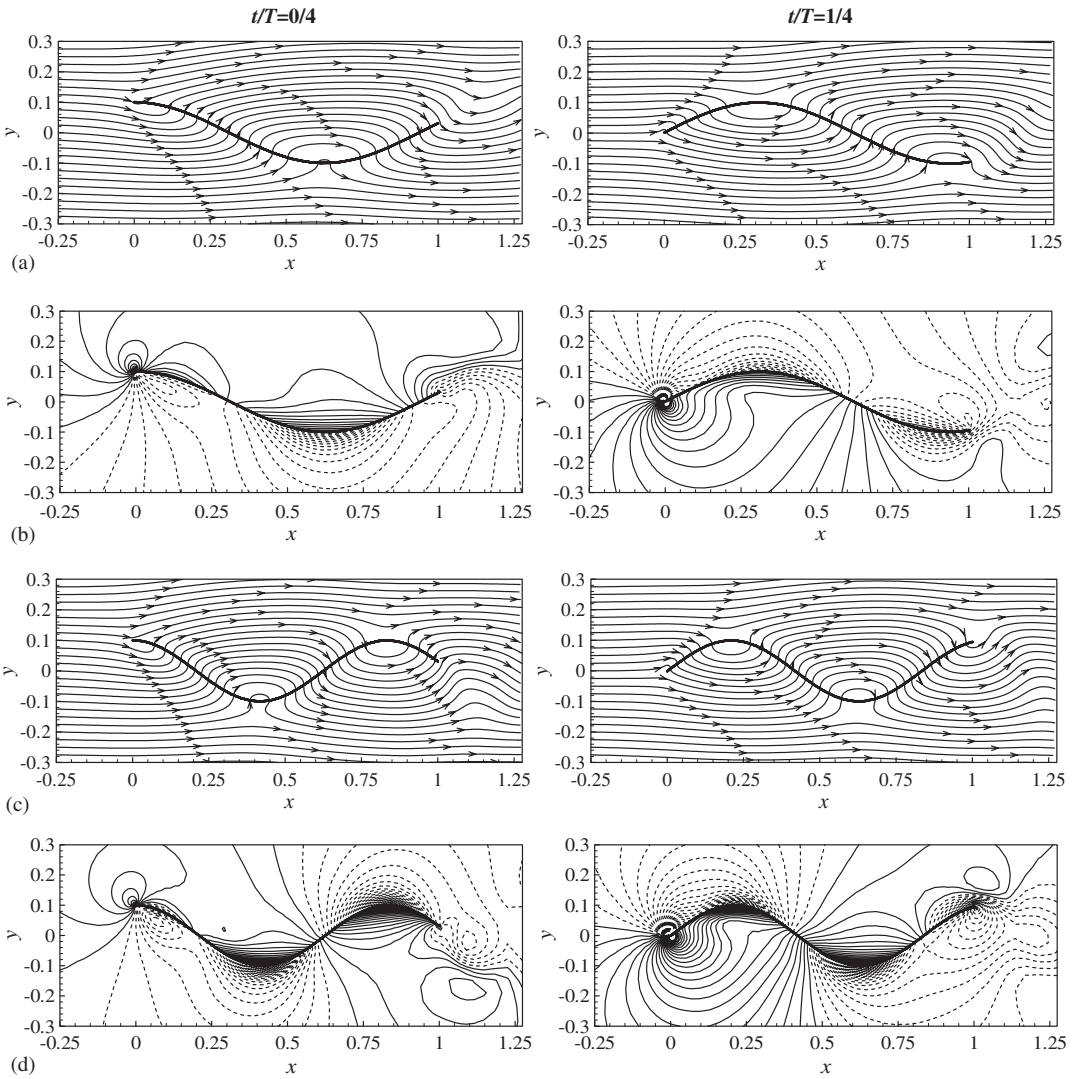

Figure 14. Instantaneous streamlines and pressure contours for $c = 1.5$ and $A_m = 0.1$ at $t/T = 0/4$ (left column) and $1/4$ (right column): (a) streamlines at $\alpha = 0.8$; (b) pressure contours at $\alpha = 0.8$; (c) streamlines at $\alpha = 1.2$; and (d) pressure contours at $\alpha = 1.2$.

increases and C_{Drms} reaches a minimum at $c = 1$. Comparing with the values for uniform amplitude in Figure 6(b), C_{Drms} and C_{Lrms} for non-uniform amplitude are relatively small for the same c.

The streamline and pressure patterns are shown in Figures 16 and 17, respectively, for several phase speeds at $t/T = 0/4$ and $1/4$. As the wavy plate is travelling in the x-direction with increasing amplitude, the vertical flow induced by the plate waving motion increases with x. Based on the analysis described above, the rear part of the travelling wavy plate thus

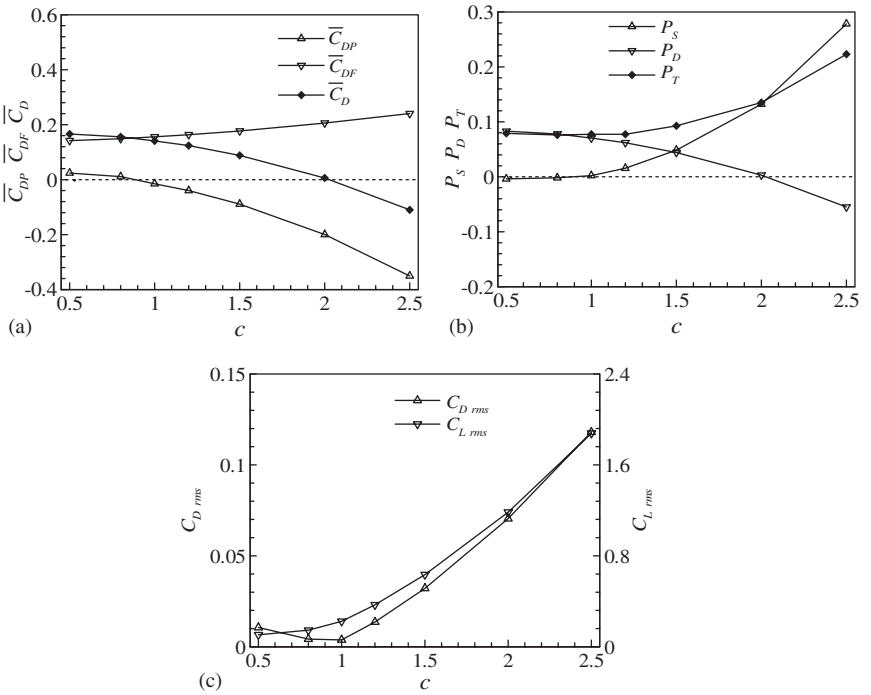

Figure 15. Time-averaged drag force and power consumption, and the rms values of drag and lateral forces for the travelling wavy wall with non-uniform amplitude: (a) drag force; (b) power consumption; and (c) C_{Drms}, C_{Lrms}.

plays an important role for propulsive performance and vortex shedding. It is evident that the flow structure exhibits remarkable change for different phase speeds. The corresponding vortex structures in the near wake of the plate are also examined and have a similar behaviour shown in Figure 10.

4.6. Comparison between the travelling wavy plate and fish swimming

To clarify the wavy motions characterizing steady undulatory swimming in fish, Videler [12] proposed some simple models to analyse the fish-like swimming motions. As an extension of the kinematics analysis, as carried out in the present study, the undulating wave motion, similar to the backbone undulation of swimming fish, is modelled simply as a travelling wavy plate. Based on the present results, it is found that the travelling wavy plate can be optimized to create thrust and to minimize net power input.

It is necessary to compare the results of the travelling wavy plate obtained in this study with some typical live fish swimming. In the measurement of steadily swimming saithe and eel, the movements of saithe and eel were observed as digitized outlines from film frames [34]. The kinematic and morphometric quantities for saithe and eel are listed in Table I.

The overall flow pattern and dynamics depend strongly on the phase speed c. As c increases, the flow structure, in particular around $c = 1$, is significantly altered. The mean force and

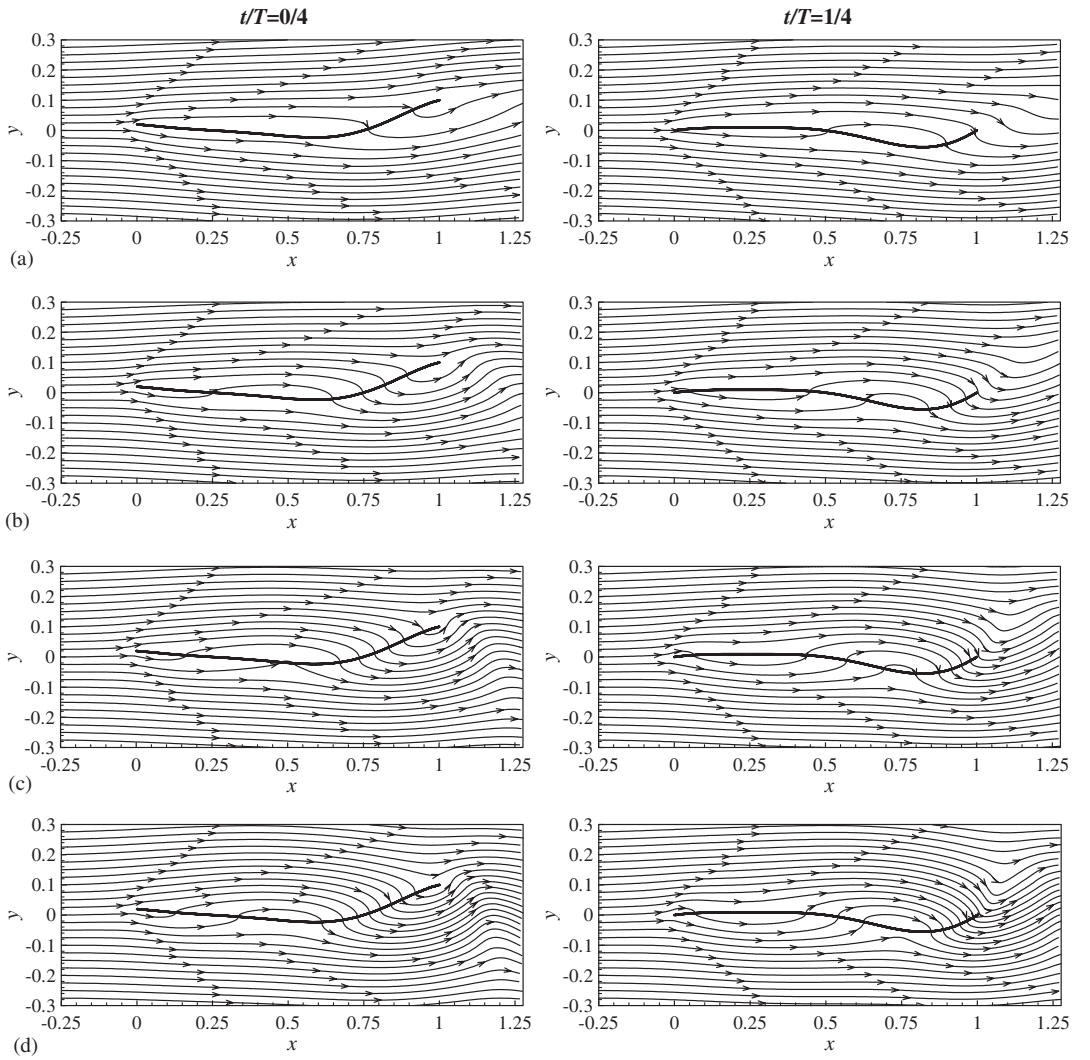

Figure 16. Instantaneous streamline patterns for the travelling wavy wall with non-uniform amplitude at $t/T = 0/4$ (left column) and $1/4$ (right column): (a) $c = 0.5$; (b) 1.0; (c) 1.5; and (d) 2.0.

power are of primary concern and are analysed above for the understanding of fish-like locomotion. Of ultimate interest is the net power required for the locomotion, which is the sum of the swimming power and the power required to overcome the total drag. This total power yields a minimum for the net power required around $c = 1.2$ approximately. As listed in Table I, the ratio of the travelling wave speed and the swimming speed V/U is 1.21 and 1.43 approximately for steadily swimming saithe and eel. Thus, it is noteworthy that $c = 1.2$–1.5 predicted numerically is the value adopted for travelling wave-like swimming motion of live fish in nature [34, 43].

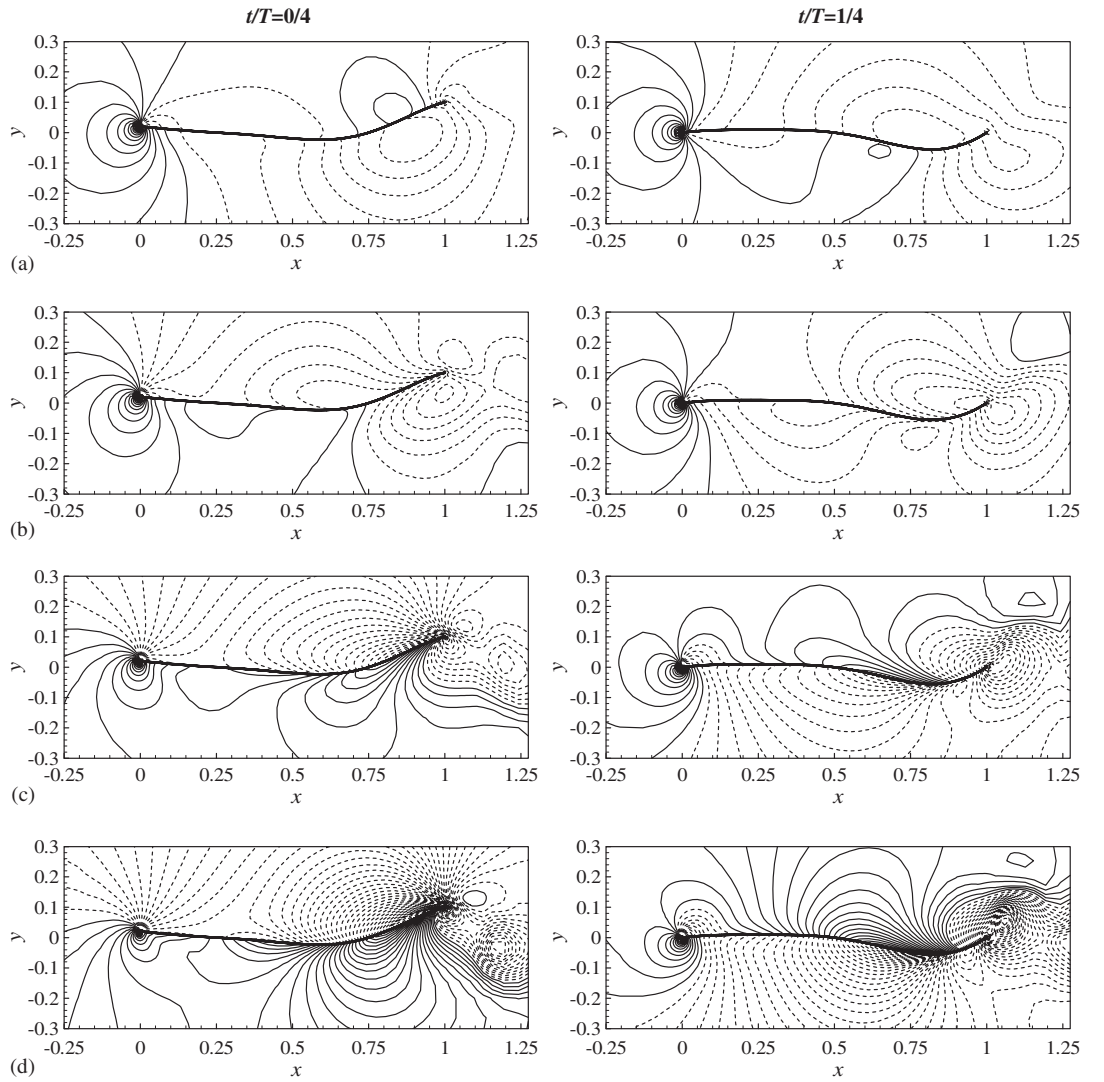

Figure 17. Instantaneous pressure contours for the travelling wavy wall with non-uniform amplitude at $t/T = 0/4$ (left column) and $1/4$ (right column): (a) $c = 0.5$; (b) 1.0; (c) 1.5; and (d) 2.0.

To elucidate effective propulsion of the travelling wavy plate, the amplitude of travelling wave is another key factor. The travelling wavy plate with uniform amplitude and with increasing amplitude is considered. As shown in Figures 11 and 12, although the wave amplitude is constant, the results are still of helpful understanding the mechanism of the propulsion for the travelling wavy plate. At larger amplitude, the wavy plate is propelled by a thrust; however, the thrust is at the expense of the swimming power P_S. On the other hand, at smaller amplitude, e.g. at $A_m = 0.05$, it is noted that, although the swimming power P_S is small, it is

Table I. Kinematic and morphometric quantities for saithe and eel [34].

Variable	Unit	Symbol	Saithe	Eel
Length	m	L	0.37	0.14
Period	s	T	0.278	0.276
Swim speed	$\mathrm{m\,s^{-1}}$	u	1.14	0.28
Relative swim speed	$L\,\mathrm{s^{-1}}$	U	3.09	2.0
Relative wave speed	$L\,\mathrm{s^{-1}}$	V	3.74	2.86
Ratio of wave speed and swim speed		V/U	1.21	1.43
Maximum tail amplitude		A/L	0.085	0.105

impossible to generate an effective thrust. Thus, based on our calculated results and previous work [25, 26], when the amplitude is around $A_m = 0.1$, an effective propulsive motion for the travelling wavy plate is reasonably generated with suitable power consumption. As listed in Table I for steadily swimming saithe and eel, the maximum tail amplitudes A/L are 0.085 and 0.105 approximately and are consistent with the proposed amplitude $A_m = 0.1$ approximately.

Based on the kinematic data of steadily swimming fish, the backbone undulation of fish swimming can be described as the travelling waves of lateral curvature with increasing amplitude [34]. As shown in Figures 15–17 for the increasing amplitude $A_m(x)$ in Figure 1(b), it is reasonably predicted that the travelling wavy plate with non-uniform amplitude is of benefit to generating a thrust. Meanwhile, C_{Drms} and C_{Lrms} for the travelling wavy plate with non-uniform amplitude are smaller that these with uniform amplitude for the same c. This feature is also helpful for fish to perform steadily swimming.

Further, it is observed that the averaged wavelength of fish swimming is the same as, and less or higher than the fish body-length for diverse fish species [34]. Thus, some typical calculations are carried out to deal with the effect of the relative wavelength α on forces and flow structures in Figures 13 and 14. Although the variations of the time-averaged drag force and power consumption for different α values considered here, as shown in Figures 13(a) and (b), are somewhat small, the influence of α on the lateral force becomes significant in Figure 13(c). Based on these results, we can qualitatively analyse saithe and eel swimming performance. Usually, steadily swimming saithe belongs to the regime of $\alpha \leqslant 1$. Large lateral force variation occurs for $\alpha \leqslant 1$; this feature is helpful for saithe to perform fast-start manoeuver swimming, in particular for C-type fast-start [45, 46]. Furthermore, swimming eel is obviously in the regime of $\alpha > 1$ [34] and mainly performs steadily swimming movements with relative small C_{Lrms} in Figure 13(c). By comparing with the typical live fish swimming, these results predicted in the present study are of helpful understanding of fish-like swimming mechanisms.

5. CONCLUDING REMARKS

The propulsive performance and vortex shedding of fish-like travelling wavy plate are numerically investigated by solving the two-dimensional incompressible Navier–Stokes equations using the finite element technique with the deforming-spatial-domain/stabilized space–time formulation. The characteristics of flow structure and vortex shedding near the travelling wavy

plate are analysed to get into physical insights to the understanding of fish-like swimming mechanisms in terms of drag reduction and optimal propulsive efficiency. The effects of some typical parameters, including the phase speed, amplitude, relative wavelength of travelling wavy plate, on the flow structures and force behaviours are discussed. The flow structures and dynamics depend strongly on the phase speed c and the amplitude A_m. The power yields a minimum around $c = 1.2$ approximately which is adopted for travelling wave-like swimming motion of live fish in nature. Effective propulsive motion for the travelling wavy plate with the amplitude around $A_m = 0.1$ is reached with suitable power consumption. The travelling wavy plate with increasing amplitude is of benefit to generating effectively propulsive performance. These parameters predicted numerically are well consistent with the available data obtained for the wave-like swimming motion of live fish in nature. On the other hand, animal locomotion is certainly far more complex and diverse than the simple model considered here. Ideally, three-dimensional computation around a flexible body is desirable and is a target in our further work.

ACKNOWLEDGEMENTS

This work was supported by the Innovation Project of the Chinese Academy of Sciences (No. KJCX-SW-L04), the National Natural Science Foundation of China (No. 10332040, 10125210), and the Program of Hundred-Talent of the Chinese Academy of Sciences.

REFERENCES

1. Lighthill MJ. Aquatic animal propulsion of high hydromechanical efficiency. *Journal of Fluid Mechanics* 1970; **44**:265–301.
2. Lighthill MJ. *Mathematical Biofluiddynamics*. SIAM: Philadelphia, PA, 1975.
3. Weis-Fogh T, Jensen M. Biology and physics of locust flight. In *Proceedings of the Royal Society Series B-Biological Science* 1956; **239**:415–585.
4. Wu TY. *Swimming and Flying in Nature*. Reinhold Publisher Corporation: New York, 1975.
5. Maxworthy T. The fluid dynamics of insect flight. *Annual Review of Fluid Mechanics* 1981; **13**:329–354.
6. Wu TY. On theoretical modeling of aquatic and aerial animal locomotion. *Advances in Applied Mechanics* 2001; **38**:291–353.
7. Phlips PJ, East RA, Pratt NH. An unsteady lifting line theory of flapping wings with application to the forward flight of birds. *Journal of Fluid Mechanics* 1981; **112**:97–125.
8. Triantafyllou MS, Triantafyllou GS, Gopalkrishnan R. Wake mechanics for thrust generation in oscillation foils. *Physics of Fluids* 1991; **3**:12–26.
9. Smith MJC, Wilkin PJ, Williams MH. The advances of an unsteady method in modeling the aerodynamic forces on rigid flapping wings. *Journal of Experimental Biology* 1996; **199**:1073–1083.
10. Anderson JM, Streitlien K, Barrett DS, Triantafyllou MS. Oscillating foils of high propulsive efficiency. *Journal of Fluid Mechanics* 1998; **360**:41–72.
11. Lu XY, Yang JM, Yin XZ. Propulsive performance and vortex shedding of a foil in flapping flight. *Acta Mechanica* 2003; **165**:189–206.
12. Videler JJ. Swimming movements, body structure and propulsion in cod Gadus morhua. In *Vertebrate Locomotion*, Day MH (ed.). Academic Press: London, 1981; 1–27.
13. Gray J. Studies in animal locomotion: I. The movement of fish with special reference to the eel. *Journal of Experimental Biology* 1933; **10**:88–104.
14. Carling J, Williams TL, Bowtell G. Self-propelled anguilliform swimming: simultaneous solution of the two-dimensional Navier–Stokes equations and Newton's laws of motion. *Journal of Experimental Biology* 1998; **201**:3143–3166.
15. Anderson EJ, McGillis WR, Grosenbaugh MA. The boundary layer of swimming fish. *Journal of Experimental Biology* 2001; **204**:81–102.
16. Liao JC, Beal DN, Lauder GV, Triantafyllou MS. The Karman gait: novel body kinematics of rainbow trout swimming in a vortex sheet. *Journal of Experimental Biology* 2003; **206**:1059–1073.
17. Gray J. Studies in animal locomotion. *Journal of Experimental Biology* 1936; **13**:192–199.

18. Wu TY. Swimming of a waving plate. *Journal of Fluid Mechanics* 1961; **10**:321–344.
19. Wu TY. Hydromechanics of swimming propulsion. Part 1. Swimming of a two dimensional flexible plate at variable forward speeds in an inviscid fluid. *Journal of Fluid Mechanics* 1971; **46**:337–355.
20. Cheng JY, Zhuang LX, Tong BG. Analysis of swimming 3-D waving plate. *Journal of Fluid Mechanics* 1991; **232**:341–355.
21. Harper DG, Blake RW. Fast-start performance of rainbow trout (Salmo gairdneri) and Northern Pike (Esox Lucius). *Journal of Experimental Biology* 1990; **150**:321–342.
22. Harper DG, Blake RW. Prey capture and the fast-start performance of northern pike Esox lucius. *Journal of Experimental Biology* 1991; **155**:175–192.
23. Barrett DS, Triantafyllou MS, Yue DKP, Grosenbaugh MA, Wolfgang MJ. Drag reduction in fish-like locomotion. *Journal of Fluid Mechanics* 1999; **392**:183–212.
24. Triantafyllou MS, Triantafyllou GS, Yue DKP. Hydrodynamics of fishlike swimming. *Annual Review of Fluid Mechanics* 2000; **32**:33–53.
25. Shen L, Zhang X, Yue DKP, Triantafyllou MS. Turbulent flow over a flexible wall undergoing a streamwise travelling wave motion. *Journal of Fluid Mechanics* 2003; **484**:197–221.
26. Lu XY, Yin XZ. Propulsive performance of a fish-like travelling wavy wall. *Acta Mechanica* 2005; **175**:197–215.
27. Tokumaru PT, Dimotakis PE. Rotary oscillation control of a cylinder wake. *Journal of Fluid Mechanics* 1991; **224**:77–90.
28. Lu XY, Sato J. A numerical study of flow past a rotationally oscillating circular cylinder. *Journal of Fluids and Structures* 1996; **10**:829–849.
29. Lu XY. Numerical study of the flow behind a rotary oscillating circular cylinder. *International Journal of Computational Fluid Dynamics* 2002; **16**:65–82.
30. Taneda S, Tomonari Y. An experiment on the flow around a waving plate. *Journal of the Physical Society of Japan* 1974; **36**:1683–1689.
31. Kendall JM. The turbulent boundary layer over a wall with progressive surface waves. *Journal of Fluid Mechanics* 1970; **41**:259–281.
32. De Angelis V, Lombardi P, Banerjee S. Direct numerical simulation of turbulent flow over a wavy wall. *Physics of Fluids* 1997; **9**:2429–2442.
33. Calhoun RJ, Street RL. Turbulent flow over a wavy surface: neutral case. *Journal of Geophysical Research* 2001; **106**:9277–9293.
34. Videler JJ. *Fish Swimming*. Chapman & Hall: New York, 1993.
35. Tezduyar TE, Behr M, Liou J. A new strategy for finite element computation involving moving boundaries and interfaces—The deforming-spatial-domain/space–time procedure: I. The concept and the preliminary numerical tests. *Computer Methods in Applied Mechanics and Engineering* 1992; **94**:339–351.
36. Brooks AN, Hughes TJR. Streamline-Upwind/Petrov–Galerkin formulation for convection dominated flows with particular emphasis on incompressible Navier–Stokes equations. *Computer Methods in Applied Mechanics and Engineering* 1982; **32**:199–259.
37. Tezduyar TE, Mittal S, Ray SE, Shin R. Incompressible flow computations with bilinear and linear equal-order-interpolation velocity-pressure elements. *Computer Methods in Applied Mechanics and Engineering* 1992; **95**:221–242.
38. Mittal S, Kumar V. Flow-induced oscillations of two cylinders in tandem and staggered arrangements. *Journal of Fluids and Structures* 2000; **15**:717–736.
39. Saad Y, Schultz M. GMRES: a generalized minimal residual algorithm for solving nonsymmetric linear systems. *SIAM Journal on Scientific and Statistical Computing* 1986; **7**:856–869.
40. Liao Q, Dong GJ, Lu XY. Vortex formation and force characteristics of a foil in the wake of a circular cylinder. *Journal of Fluids and Structures* 2004; **19**:491–510.
41. Dong GJ, Lu XY, Zhuang LX. Discontinuity-capturing finite element computation of unsteady flow with adaptive unstructured meshes. *Acta Mechanica Sinica* 2004; **20**:347–353.
42. McHenry MJ, Azizi E, Strother JA. The hydrodynamics of locomotion at intermediate Reynolds numbers: undulatory swimming in ascidian larvae (*Botrylloides* sp.). *Journal of Experimental Biology* 2003; **206**: 327–343.
43. Videler JJ, Hess F. Fast continuous swimming of two pelagic predators, saithe (pollachius virens) and mackerel (scomber scombrus): a kinematic analysis. *Journal of Experimental Biology* 1984; **109**:209–228.
44. Li XM, Lu XY, Yin XZ. Visualization on fish's wake. *Proceedings of the Society of Photo-Optical Instrumentation Engineers* 2002; **4537**:473–476.
45. Domenici P, Blake RW. The kinematics and performance of fish fast-start swimming. *Journal of Experimental Biology* 1997; **200**:1165–1178.
46. Ahlborn B, Chapman S, Stafford R, Blake RW, Harper DG. Experimental simulation of the thrust phases of fast-start swimming of fish. *Journal of Experimental Biology* 1997; **200**:2301–2312.

